

See discussions, stats, and author profiles for this publication at: <https://www.researchgate.net/publication/262388265>

# Oligo(p-phenyleneethynylene) Derived Porous Luminescent Nanoscale Coordination Polymer of GdIII: Bimodal Imaging and Nitroaromatic Sensing

ARTICLE *in* THE JOURNAL OF PHYSICAL CHEMISTRY C · MAY 2014

Impact Factor: 4.77 · DOI: 10.1021/jp501030h

---

CITATIONS

5

READS

59

---

## 7 AUTHORS, INCLUDING:



SNEHAJYOTI CHATTERJEE

University of Pennsylvania

21 PUBLICATIONS 136 CITATIONS

[SEE PROFILE](#)



Rahul Modak

KIIT University

14 PUBLICATIONS 169 CITATIONS

[SEE PROFILE](#)



Vivek Tiwari

Centre for Cellular and Molecular Biology

15 PUBLICATIONS 48 CITATIONS

[SEE PROFILE](#)



Tapas Maji

Jawaharlal Nehru Centre for Advanced Scien...

176 PUBLICATIONS 4,261 CITATIONS

[SEE PROFILE](#)

# Oligo(*p*-phenyleneethynylene)-Derived Porous Luminescent Nanoscale Coordination Polymer of Gd<sup>III</sup>: Bimodal Imaging and Nitroaromatic Sensing

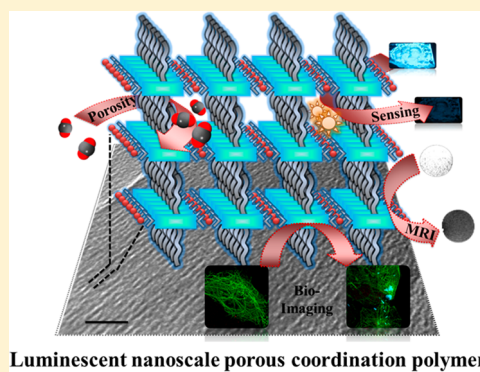
Venkata M. Suresh,<sup>†</sup> Snehajyoti Chatterjee,<sup>‡</sup> Rahul Modak,<sup>‡</sup> Vivek Tiwari,<sup>§</sup> Anant B. Patel,<sup>§</sup> Tapas K. Kundu,<sup>‡</sup> and Tapas Kumar Maji\*,<sup>†</sup>

<sup>†</sup>Molecular Materials Laboratory, Chemistry and Physics of Materials Unit, and <sup>‡</sup>Transcription and Disease Laboratory, Molecular Biology and Genetics Unit, Jawaharlal Nehru Centre for Advanced Scientific Research (JNCASR), Jakkur, Bangalore, India 560064

<sup>§</sup>NMR Microimaging and Spectroscopy, Centre for Cellular & Molecular Biology, Uppal Road, Hyderabad, India 500007

## Supporting Information

**ABSTRACT:** Self-assembled highly luminescent nanoscale coordination polymer of  $\{[\text{Gd}(\text{OPE})(\text{NO}_3)(\text{H}_2\text{O})_2]\cdot\text{H}_2\text{O}\}$  (NCP-1), (oligo-(*p*-phenyleneethynylene)dicarboxylate) was synthesized by coordination-driven self-assembly of oligo-(*p*-phenyleneethynylene)dicarboxylic acid and Gd<sup>III</sup> in polar solvent under refluxing conditions. This nanostructure has been characterized by FESEM, TEM, powder X-ray diffraction, and adsorption study. Interdigitation between 1D coordination polymers through alkyl chains results in a porous supramolecular 3D extended structure. NCP-1 shows permanent microporosity as revealed by type-I CO<sub>2</sub> uptake profile. FESEM and TEM studies of NCP-1 reveal nanorod-like morphology with square-type cross section having dimensions of 50–100 nm diameter and 0.5–0.8 μm length. High-magnification TEM images show long-range structural ordering present in NCP-1 with uniform dark lines having an interspacing distance of 0.9–1.1 nm. Physiological stability and strong luminescence features of NCP-1 have been exploited for bioimaging based on internalization into mammalian cultured cell lines HEK 293T and H1299. Magnetic resonance imaging studies suggest that NCP-1 could act as a potential negative (T<sub>2</sub>) contrast agent. Furthermore, this porous luminescent NCP-1 shows efficient nitroaromatic sensing as realized by the fluorescence quenching in solution as well as in vapor phase of the analyte like 2,4-dinitrotoluene (2,4-DNT). These results demonstrate that hybridization of a paramagnetic metal center and luminescent linker in a nanoscale porous coordination polymer culminates in a functional hybrid material with potential bimodal imaging and sensing applications.



Luminescent nanoscale porous coordination polymer

## INTRODUCTION

Porous coordination polymers (PCPs)<sup>1–7</sup> are a class of crystalline materials constructed by the self-assembly of metal ions and polydentate organic linkers with a wide range of modular pore size and surface area and have been extensively studied for applications in gas storage,<sup>8–13</sup> separation,<sup>14–18</sup> sensing,<sup>19–21</sup> drug delivery,<sup>22–25</sup> optical properties,<sup>26–28</sup> and catalysis.<sup>29–32</sup> The recent upsurge in synthesis of PCPs stems from their functional behavior with a set of well-defined properties such as magnetism and porosity, photoluminescence and magnetism, conductivity and luminescence, and luminescence and porosity in a single framework system.<sup>33–41</sup> The presynthetic design strategies like judicious choice of building blocks and suitable reaction conditions can address the challenges of synthesizing such functional hybrid materials. For example, Veciana et al. reported highly porous magnetic framework  $\{\text{Cu}_3(\text{PTMTC})_2(\text{py})_6(\text{CH}_3\text{CH}_2\text{OH})_2(\text{H}_2\text{O})\}$  using polychlorinated triphenylmethyl radical functionalized with three carboxylic acids (PTMTC) as a bridging linker that reveals guest responsive change in magnetic properties.<sup>42</sup>

In this context, design and synthesis of luminescent porous coordination polymers with suitable chromophoric linkers and metal ions and their potential applications in different fields is yet to be properly explored. Particularly the hydrolytic instability or bulk crystalline phase of most of the PCPs limits their applications in biomedical and biological fields.<sup>43</sup> Therefore, luminescent nanoscale coordination polymers (NCPs) with uniform size and morphologies<sup>44,45</sup> are highly promising in designing functional nanomaterials for multimodal imaging and drug delivery applications based on their easy internalization into cells.<sup>46–50</sup> Nanoscale dimensions of these inherent microporous materials would enhance solution processability that would help in fabrication of thin film devices and sensors.<sup>51–58</sup> Recently, Lin et al. reported BODIPY grafted Fe<sup>III</sup>-carboxylate  $[\text{Fe}_3(\mu_3-\text{O})\text{Cl}(\text{H}_2\text{O})_2(\text{NH}_2-\text{BDC})_3]$  nanoparticles as delivery vehicles and optical imaging agents.<sup>59</sup>

Received: January 29, 2014

Revised: May 1, 2014

They have also reported nanorods of  $\{\text{Gd}(\text{BDC})_{1.5}(\text{H}_2\text{O})_2\}$  for magnetic resonance imaging (MRI) with high relaxivity, and further doping with  $\text{Tb}^{3+}$  and  $\text{Eu}^{3+}$  of the Gd-nanorods multimodal imaging application was realized.<sup>60</sup> However, NCPs based on a MRI active metal ion and a highly luminescent organic linker are yet to be explored, and such hybrid material would offer a unique class of multifunctional material for potential applications in multimodal imaging, drug delivery, and sensing. With this objective we envision the design and synthesis of functional hybrid nanostructure based on a luminescent  $\pi$ -conjugated linker and Gd<sup>III</sup> paramagnetic metal center. In our design, we have self-assembled oligo-(*p*-phenyleneethynylene)dicarboxylic acid (OPEA) with soluble alkyl chains on both ends and Gd<sup>III</sup> metal ion into a new luminescent nanoscale coordination polymer  $\{[\text{Gd}(\text{OPE})-(\text{NO}_3)(\text{H}_2\text{O})_2]\cdot\text{H}_2\text{O}\}$  (NCP-1). This NCP-1 is characterized by several spectroscopic and microscopic techniques and has been studied for properties like nitroaromatic sensing and bimodal imaging based on a luminescent OPEA linker and MRI active Gd<sup>III</sup> metal ion.

## ■ EXPERIMENTAL SECTION

**Materials and Measurements.** Tetrakis(triphenylphosphine)palladium(0), copper iodide ( $\text{CuI}$ ), and  $\text{Gd}(\text{NO}_3)_3\cdot 6\text{H}_2\text{O}$  were purchased from Sigma-Aldrich Chemical Co. Oligo-(*p*-phenyleneethynylene)dicarboxylic acid (OPEA) is synthesized using literature procedures.<sup>61,62</sup> Required solvents were dried prior to use. Elemental analysis was carried out using a Thermo Scientific Flash 2000 CHN analyzer. Infrared spectral studies were done by making samples with KBr pellets using a Bruker FT-IR spectrometer. Thermal stability of coordination polymer was analyzed using a Mettler Toledo TGA 850 instrument under inert atmosphere in the temperature range of 30–800 °C at a heating rate of 5 °C per min. Powder X-ray diffraction studies of the samples were recorded on a Bruker D8 discover instrument using Cu- $\text{K}\alpha$  radiation. Morphological studies have been carried out using a Lica-S440I field emission scanning electron microscope (FESEM) by placing samples on a silicon wafer under high vacuum with an accelerating voltage of 10 kV. Transmission electron microscopy (TEM) analysis has been performed using JEOL JEM-3010 with an accelerating voltage at 300 kV. For this analysis NCP-1 is dispersed in ethanol by sonication before drop casting on a carbon-coated copper grid. Porosity measurements were carried out using a QUNATACHROME QUADRASORD-SI analyzer at 77 K for  $\text{N}_2$  and 195 K for  $\text{CO}_2$ . Fluorescence studies were accomplished using a PerkinElmer LS 55 Luminescence spectrometer.  $^1\text{H}$  NMR is recorded on a Bruker AV-400 spectrometer with chemical shifts reported as parts per million. T1 and T2 measurements were carried out at 25 °C using a vertical wide bore (89 mm) 14.1 T magnet interfaced with Avance II Microimager (Bruker Biospin, Germany) equipped with 60 mm actively shielded gradient. Nanorods were dispersed in 0.5% agarose at different concentration and placed into a 0.7 mL microfuge tube. Axial images of the microfuge tube filled with nanorod dispersed in agarose were acquired for the relaxation time measurements. The typical parameters used for T1 measurements are echo time (TE) = 7 ms; repetition time (TR) = varies from 250 to 15 000 ms; slice thickness = 0.5 mm; field of view = 15 mm × 15 mm; matrix size = 64 × 64. The T1 value was determined by fitting the function  $S_{\text{TR}} = S_{\text{TR}(\infty)}(1 - \exp(-\text{TR}/\text{T1}))$  to the signal intensity versus repetition time graph, where  $S_{\text{TR}(\infty)}$

represents MR intensity at infinite repetition time. The parameters used for the T2 measurements were TR = 10 000 ms and TE varying between 10 and 320 ms. All other parameters used were the same as that of the T1 measurements. The T2 value was obtained by fitting the function  $S_{\text{TE}} = S_{\text{TE}(0)} \exp(-\text{TE}/\text{T2}))$  to the signal intensity versus echo time graph, where  $S_{\text{TE}(0)}$  represents MR intensity with zero echo time. The longitudinal ( $r_1$ ) and transverse relaxivity ( $r_2$ ) of the nanorods were calculated from the slope of  $R1(1/\text{T1})/R2(1/\text{T2})$  versus concentration graph.

**Cell Culture.** HEK293T and H1299 cells were grown in the presence of a Dulbecco modified Eagle medium (DMEM) supplemented with 10% fetal bovine serum at 37 °C in a 5%  $\text{CO}_2$  incubator.

**Immunofluorescence in Cell Line.** Immunofluorescence with confocal microscopy was performed as described elsewhere.<sup>63</sup> Briefly, HEK293T or H1299 cells were grown on poly-L-lysine coated coverslips at 37 °C in a 5%  $\text{CO}_2$  incubator to 30–50% confluence, and 40  $\mu\text{g}$  of NCP-1 was added. After the indicated time points, the coverslips containing adhered cells were washed with 1× phosphate buffer saline (PBS) fixed using 4% paraformaldehyde followed by permeabilization with Triton-X 100. Nonspecific antigens were blocked with FBS, and appropriate dilution of antitubulin primary antibody was added. The secondary antibody was fluorescently tagged and was used with appropriate dilution. Washes with buffer were performed after each step. Images were taken with Carl Zeiss LSM 510 META laser scanning confocal microscope.

**Synthesis of  $\{[\text{Gd}(\text{OPE})(\text{NO}_3)(\text{H}_2\text{O})_2]\cdot\text{H}_2\text{O}\}$ , (NCP-1).**  $\text{Gd}(\text{NO}_3)_3\cdot 6\text{H}_2\text{O}$  (1 equiv, 14 mg) was dissolved in 5 mL of dimethylformamide (DMF) and added dropwise to OPEA (1 equiv, 25 mg) solution in DMF at 140 °C and stirred for 30 min. The reaction mixture was cooled to room temperature, and then a mixture of ethanol/water (1:1) was added that resulted in a colloid formation. These colloids were centrifuged and thoroughly washed with ethanol and dried under vacuum for 6 h. The resultant products were characterized by different techniques. Yield: 54%. Elemental analysis for  $\text{GdC}_{40}\text{H}_{50}\text{NO}_{12}$ . Calcd: C, 53.7; H, 5.6; N, 1.5. Found: C, 54.2; H, 5.6; N, 1.6. FTIR in KBr ( $\text{cm}^{-1}$ ): 3357(br), 2925(sh), 2854(sh), 2670(w), 2543(w), 2208(w), 1689(vs), 1602(s), 1531(m), 1417(s), 1382(vs), 1282(m), 1216(w), 1178(w), 1018(w), 862(w), 773(w).

## ■ RESULTS AND DISCUSSION

**Structural Characterization.** Oligo(*p*-phenyleneethynylene)dicarboxylic acid with octyloxy (C8) chains on both sides is synthesized through the Sonogashira coupling strategy (Supporting Information Figure S1). DMF solution of  $\text{Gd}(\text{NO}_3)_3\cdot 6\text{H}_2\text{O}$  (1 equiv) is added to OPEA (1 equiv) ligand and heated at 140 °C for 30 min and then cooled to room temperature. Slow addition of EtOH/H<sub>2</sub>O (1:1) to the reaction mixture at room temperature results in a colloidal solution. These colloids were collected by centrifugation, washed with ethanol, and dried under vacuum at room temperature for 6 h. The compound is further characterized by elemental analysis, Fourier transform infrared spectroscopy (FTIR), powder X-ray diffraction (PXRD), thermogravimetric analysis (TGA), field-emission scanning electron microscopy (FESEM), transmission electron microscopy (TEM), and adsorption measurements. The presence of Gd<sup>III</sup> in colloids is supported by energy dispersive X-ray analysis (EDAX) (Supporting Information Figure S2), and elemental analysis

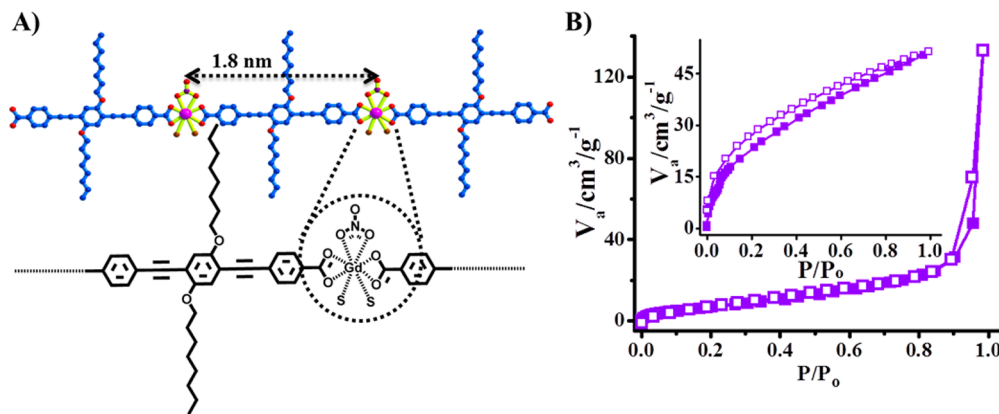


**Figure 1.** (A) Schematic representation showing coordination environment of Gd<sup>III</sup> ion in NCP-1. (B) Adsorption isotherms of NCP-1, N<sub>2</sub> at 77 K and inset showing CO<sub>2</sub> adsorption at 195 K.

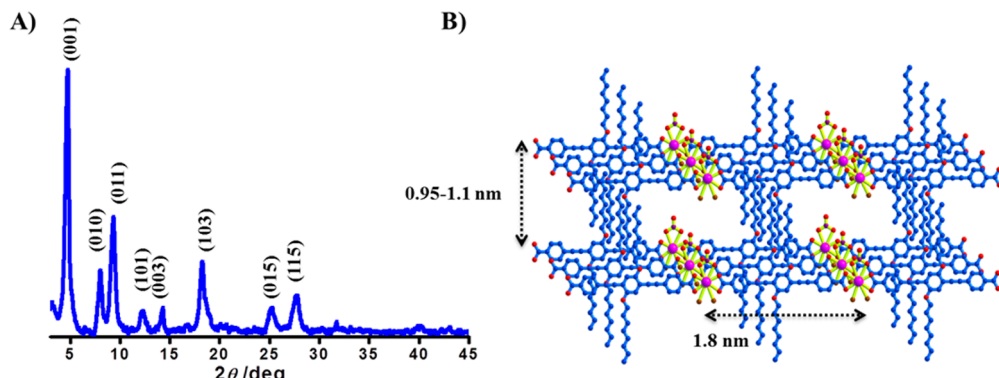


**Figure 2.** (A) PXRD pattern of NCP-1 and (B) proposed model structure of 3D interdigitated porous structure of NCP-1.

(see Experimental section) suggests a molecular formula of  $\{[\text{Gd}(\text{OPE})(\text{NO}_3)(\text{H}_2\text{O})_2]\cdot\text{H}_2\text{O}\}$ , (NCP-1) for as-synthesized compound. FTIR of NCP-1 shows strong bands at 1687 and 1525 cm<sup>-1</sup> characteristic of  $\nu_s(\text{COO})$  and  $\nu_{as}(\text{COO})$  of OPE linker connected to Gd<sup>III</sup> center (Supporting Information Figure S3). The presence of strong signal at 1385 cm<sup>-1</sup> corresponding to the  $\nu(\text{NO})$  of nitrate ion indicates its coordination to Gd<sup>III</sup> center. In addition, the remaining coordination sites in Gd<sup>III</sup> could be fulfilled by the water molecules (Figure 1A) which is supported by the broad band centered at 3560–3212 cm<sup>-1</sup>. TGA analysis shows initial weight loss (6% equal to three water molecules) in the range of 65–150 °C corresponding to loss of guest as well as coordinated water molecules (Supporting Information Figure S4), and further heating results in no weight loss until 350 °C suggesting that dehydrated compound is highly stable. Therefore, NCP-1 is activated at 150 °C before doing N<sub>2</sub> (77 K) and CO<sub>2</sub> (195 K) gas adsorption measurements. It is worth mentioning that NCP-1 is crystalline in nature, and the PXRD pattern of dehydrated NCP-1 show no changes compared to as-synthesized compound suggesting stability of framework on removal of guest molecules (Supporting Information Figure S5). Adsorption of N<sub>2</sub> (kinetic diameter = 3.64 Å) at 77 K shows a typical type-II profile suggesting NCP-1 is nonporous with respect to N<sub>2</sub> (Figure 1B). Interestingly, CO<sub>2</sub> adsorption shows sharp uptake in the low-pressure region with typical type-I profile indicating the microporous nature of NCP-1 with pore size <2 nm. The amount of the CO<sub>2</sub> uptake at the end point is found to be 52 mL/g (Figure 1B) corresponding to 2.1 CO<sub>2</sub> molecules per formula unit, and the

Langmuir surface area is calculated to be 293 m<sup>2</sup> g<sup>-1</sup>. Crystallization of OPEA and Gd(NO<sub>3</sub>)<sub>3</sub>·6H<sub>2</sub>O through several methods has failed, so the possible structure shown in Figure 2 is achieved from studies like PXRD, adsorption, and TEM as described in the literature.<sup>64–67</sup> The experimental powder diffraction pattern (Figure 2A) has been evaluated using CRYSFIRE powder indexing system using the Taup (TP) program, and the results are listed in Table 1 with unit cell

**Table 1.** Unit Cell Parameters of NCP-1<sup>a</sup>

<i>h</i>	<i>k</i>	<i>l</i>	2θ	<i>D</i> (exptl)	<i>D</i> (calcd)	max. dev.
0	0	1	4.7417	18.529 20	18.6211	0.0493
0	1	0	8.1134	10.943 96	10.8885	0.0830
0	1	1	9.4014	9.442 14	9.3995	0.0961
1	0	1	12.3617	7.188 12	7.1544	0.0126
0	0	3	14.2577	6.236 76	6.2070	0.0145
1	0	3	18.2981	4.845 29	4.8445	0.0185
0	1	5	25.2535	3.520 04	3.5238	0.0252
1	1	5	27.7894	3.208 29	3.2077	0.0275

<sup>a</sup> $V = 1571.22$  (Å<sup>3</sup>). Phase = orthorhombic. Parameters:  $a = 7.749$  27 Å,  $b = 10.888$  Å,  $c = 18.621$  Å;  $\alpha = 90^\circ$ ,  $\beta = 90^\circ$ , and  $\gamma = 90^\circ$ .

parameters, *hkl* values for different planes. Diffraction patterns suggest orthorhombic phase for NCP-1, where  $a = 7.749$  27 Å,  $b = 10.888$  6 Å, and  $c = 18.621$  1 Å and insignificant deviations in *d*-values suggest that the calculated values fitted well with experimental data. Diffraction peak in the low-angle region at 4.7° with *d*-spacing 18.6 Å corresponds to the (001) plane and can be assigned to the repetition of metal centers separated by

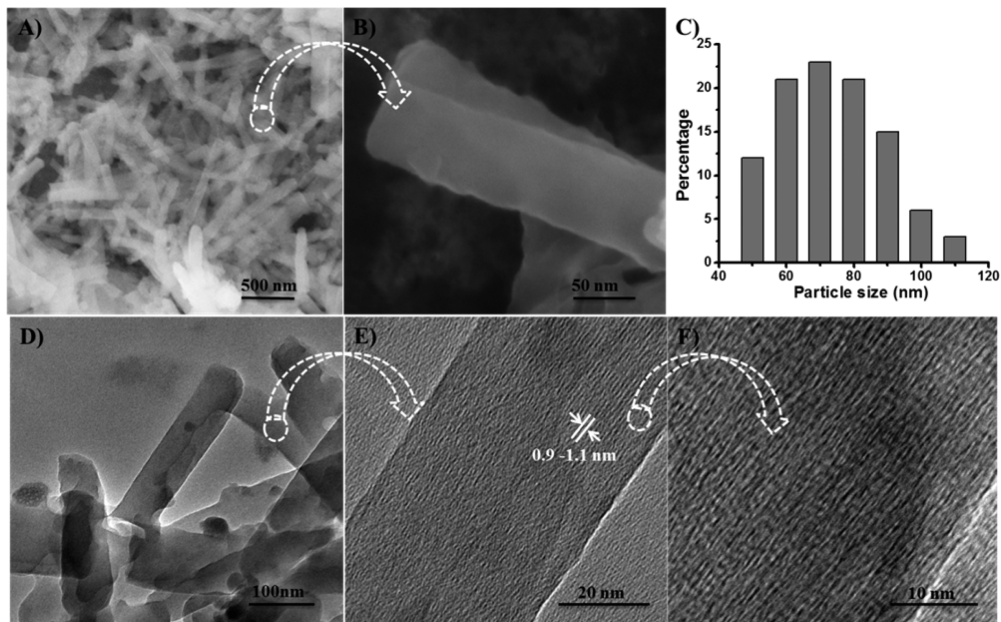


**Figure 3.** Electron microscope images of NCP-1: (A), (B) FESEM images at different magnifications and (C) particle size distribution diagram. TEM images (D) at low magnification and (E), (F) at high magnification showing dark and bright regions indicating the ordering present in NCP-1.

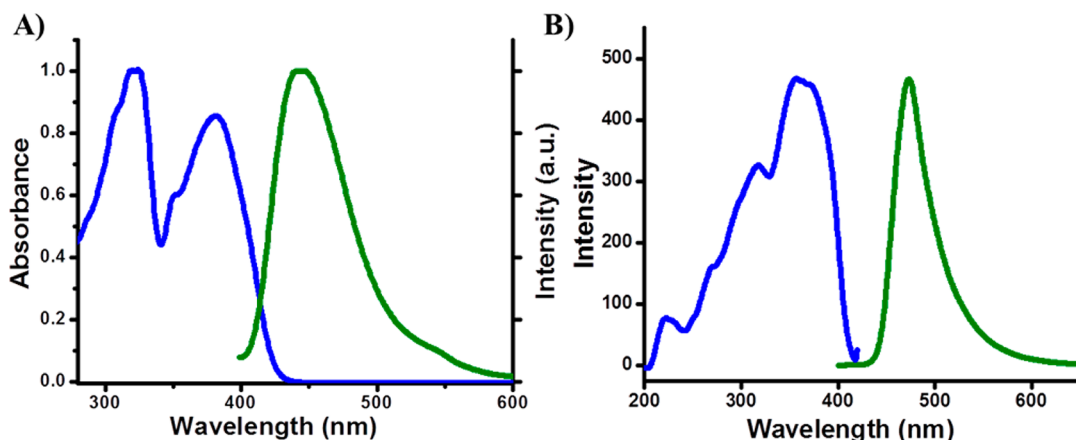


**Figure 4.** (A) Absorbance (blue) and fluorescence spectra (green) of OPEA ligand in ethanol. (B) Excitation (blue) and fluorescence spectra (green) of OPEA in solid state.

OPE linker and formation of a 1D coordination chain. Now, these 1D chains can undergo interdigitation through octyloxy (C8) side chains based on H-bonding interactions between alkyl CH and alkoxy oxygen and hydrophobic interactions to form a 2D structure, which is supported by the diffraction peak at  $2\theta$  value of  $8^\circ$  ( $d = 10.8 \text{ \AA}$ ) and is assigned to (010) plane. Interdigitation of long-chain alkoxy chains of *p*-phenyleneethynlenes is known to form through hydrogen bonding between alkyl CH and alkoxy oxygen and is documented in the literature.<sup>68</sup> We believe that these types of H-bonding interactions along with hydrophobic interactions helped to form extended interdigitated structure. This 2D network could preferably pack through weak  $\pi-\pi$  interactions of the OPE core as supported by the diffraction peak at  $27.7^\circ$  with  $d$ -spacing of  $3.6 \text{ \AA}$  and forms a 3D extended supramolecular porous structure. A proposed model of NCP-1 developed from the above results is shown in Figure 2B.

**SEM and TEM Studies.** NCP-1 is further studied by electron microscopy techniques (FESEM and TEM). As shown in Figure 3A and B, NCP-1 exhibits nanorod type morphology

with square type of cross section. Most of the nanorods show diameter ranges from 50 to 100 nm with  $0.5\text{--}0.8 \mu\text{m}$  length as shown in the particle size distribution diagram (Figure 3C). TEM studies also reveal well-defined rodlike morphology (Figure 3D) which is likely the result of preferred arrangement of several 1D coordination chains in polar solvent. Interestingly, TEM of these nanorods at higher magnification shows clear ordering present in NCP-1 with equally distant dark lines throughout the nanorod (Figure 3E, F). Interspacing measured between two successive dark lines is found to be  $0.95\text{--}1.1 \text{ nm}$ , which is in good agreement with the  $d$ -spacing ( $1.08 \text{ nm}$ ) calculated from the PXRD pattern. These observations unequivocally suggest the interdigitation of 1D coordination chains. Furthermore, the microporous nature of NCP-1 obtained from type-I  $\text{CO}_2$  profile can be correlated with the porosity created due to the interdigitation of alkyl chains in NCP-1. Therefore, the hydrophobic and H-bonding interactions between alkyl chains in polar solvents drive the formation of a 3D interdigitated supramolecular microporous structure.

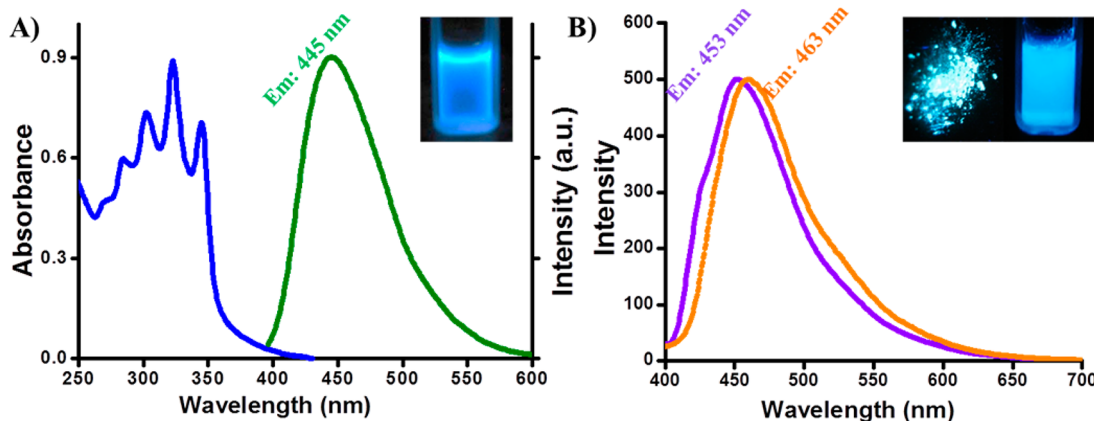


**Figure 5.** (A) Absorbance (blue) and fluorescence spectra (green) of NCP-1 dispersed in ethanol. (B) Fluorescence spectra of NCP-1 in PBS buffer (violet) and solid state (orange). Inset: Images of NCP-1 in ethanol (left), solid state and PBS dispersion (right) under UV light, respectively.

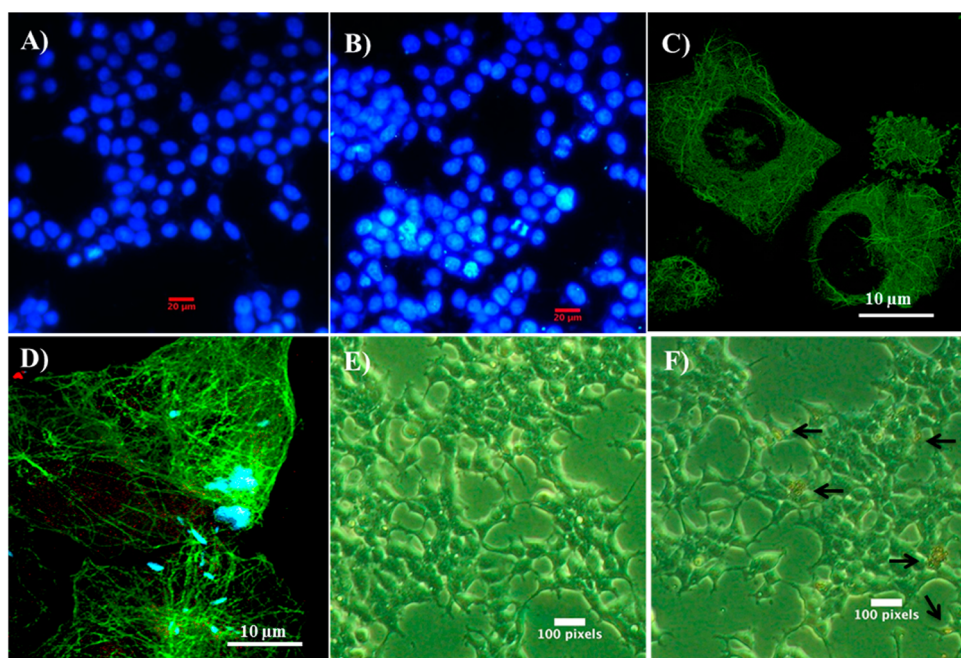


**Figure 6.** Fluorescence microscope images of HEK 293T cells (A) before and (B) after treating with nanoparticles of NCP-1 showing its nontoxicity. Blue color represents nucleus (DAPI staining), and the cyan color represents NCP-1. (C), (D) confocal microscope images of H1299 cells before and after treating with nanoparticles of NCP-1 respectively. Green color represents cell cytoskeleton (tubulin staining), and the cyan color represents NCP-1. Inverted microscopic images of H1299 cells (E) before and (F) after treatment with NCP-1. Arrows indicates the nanoparticles.

**Photoluminescent Properties of NCP-1: Bimodal Imaging.** Oligo-(*p*-phenyleneethynylene)dicarboxylic acid (OPEA) with alkyl chains on both sides shows high solubility in polar solvents like tetrahydrofuran, ethanol, *N,N*'-dimethylformamide (DMF), and dimethyl sulfoxide (DMSO). Ethanolic solution of OPEA shows strong blue emission ( $\lambda_{\text{em}} = 440 \text{ nm}$ ) when excited at 330 nm (Figure 4A) and strong cyan emission at 473 nm (Figure 4B) in solid state when excited at 390 nm. On the other hand, NCP-1 forms stable colloid in DMF, and no precipitation is observed for several months suggesting the significant solution processability of NCP-1 colloids. Similar to OPEA, ethanol dispersion of NCP-1 showed strong linker-based blue emission ( $\lambda_{\text{em}} = 445 \text{ nm}$ ) on 330 nm excitation and intense cyan emission ( $\lambda_{\text{em}} = 463 \text{ nm}$ ,  $\lambda_{\text{ex}} = 390 \text{ nm}$ ) in solid state (Figure 5, Supporting Information Figure S6).

Strong emission features of porous NCP-1 prompted us to study the internalization of these nanostructures into mammalian cells for bioimaging applications. Before doing optical imaging studies, NCP-1 is tested for its hydrolytic stability under physiological conditions. Incubation of nanorods of NCP-1 in PBS buffer for 12 h shows no considerable changes in emission properties ( $\lambda_{\text{em}} = 453 \text{ nm}$ ,  $\lambda_{\text{ex}} = 390 \text{ nm}$ , only L in PBS emit at 473 on 390 nm excitation) suggesting the stability of NCPs in physiological conditions (Figure 5B, Supporting Information Figure S7). Further, the stability of NCPs is studied using X-ray diffraction measurements. Supporting Information Figure S8 shows the diffraction pattern of NCPs incubated in PBS compared with as-synthesized NCPs; all the diffraction peaks characteristic of NCP-1 are retained in the PBS incubated NCP-1 suggesting its stability under physiological conditions. Further, EDAX analysis of

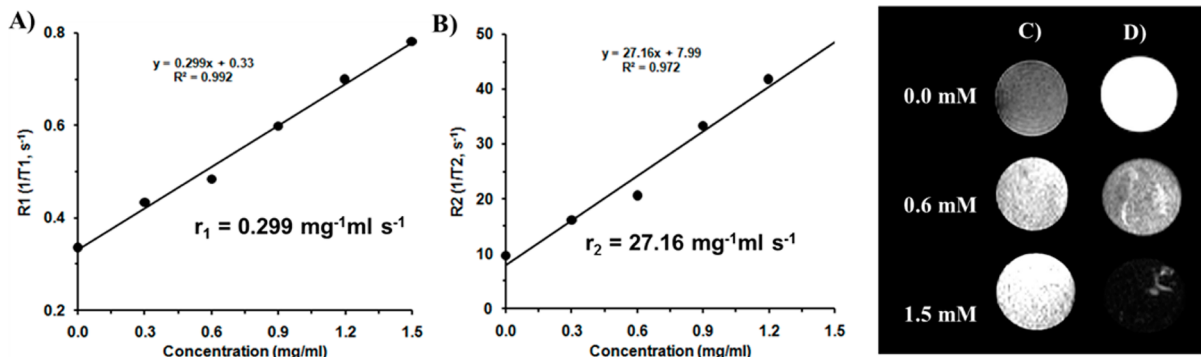


**Figure 7.** Variation of (A)  $R_1$  and (B)  $R_2$  of water with increasing concentration of nanorods of NCP-1. The slope of the line represents the corresponding relaxivity. (C) T1- and (D) T2-weighted MR images of microfuge containing NCP-1 in 0.5% agarose.

decant obtained from PBS incubated NCP-1 shows no leaching of  $\text{Gd}^{III}$  ion into the PBS solution (Supporting Information Figure S9). Further, ICP analysis of decant from NCP-1/PBS showed nearly 0.3 ppm which is a very feeble amount of  $\text{Gd}^{III}$  ion present in the solution, indicating no significant decomposition of NCP-1 in PBS. In order to study the cell permeability of NCP-1, we selected human embryonic kidney cell line HEK 293T and human nonsmall cell lung carcinoma cell line H1299. The cells were grown up to 30–50% confluence for the cell membrane permeabilization study. NCP-1 (40  $\mu\text{g}$ ) suspended in buffer was added to cells adhered on a 30 mm dish HEK and incubated for 12 h. By virtue of its self-fluorescence, we studied the distribution of NCP-1 in the above-mentioned cell lines. Surprisingly, we observed appreciable distribution of NCP-1 throughout 293T cells evidenced through confocal imaging (Figure 6A, B). Immunofluorescence using antitubulin antibody also suggested the internalization of NCP-1 within the cytoplasm of H1299 cells further strengthening its potential to cross cell membranes (Figure 6C, D). It is expected that the nanorods enter the cell line longitudinally due to their nanoscale dimension of width (50–100 nm). Interestingly, no floating or dead cells were observed even after 24 h of treatment signifying nontoxic effect of NCP-1 upon cellular internalization (Figure 6E, F). These results suggest that high-stability, less toxic nanostructures of NCP-1 can be satisfactorily internalized into cells for bioimaging applications under physiological conditions.

Magnetic resonance imaging (MRI) is an immensely valuable noninvasive technique used in diagnostic clinical imaging to obtain temporal information with significantly improved resolution. Changes in the longitudinal ( $T_1$ ) and transverse ( $T_2$ ) relaxations of water protons from different tissues alter the signal intensities in MR imaging. Administration of contrast agent changes the signal intensity by decreasing the relaxation rate of mobile water protons in tissue. Nanocarriers containing contrast agents like  $\text{Gd}^{III}$ -chelates have been used for MR imaging applications.<sup>69</sup> The well-defined nanorod-like morphology, the presence of large number of periodically aligned  $\text{Gd}^{III}$  ions, high biological stability, excellent cell permeability, and luminescence imaging properties of NCP-1 could mark it as a potential bimodal MRI/optical imaging probe. To check the efficiency of NCP-1 as a contrast agent,  $T_1$  and  $T_2$  relaxation times were measured using a vertical wide bore (89 mm) 14.1 T NMR Microimager at 25 °C. In a typical experiment, aqueous suspension of NCP-1 in 0.5% agarose is tested for longitudinal and transverse relaxation times with different concentration of NCP particles (0.0, 0.6, and 1.5 mM).

Relaxivities  $r_1$  ( $0.3 \text{ s}^{-1}/\text{mM}$ ) and  $r_2$  ( $27.9 \text{ s}^{-1}/\text{mM}$ ) were measured by plotting  $1/T_1$  and  $1/T_2$  respectively against concentration of NCP-1 (Figure 7A, B). The relaxivities ratio  $r_2/r_1$  is found to be higher (95) than reported Prussian blue nanoparticles and comparable to iron oxide nanoparticles.<sup>70,71</sup> High  $r_2/r_1$  ratio value clearly indicates that NCP-1 has high potential as a  $T_2$  contrast agent, and recently Gd-containing gels and complexes have been demonstrated as negative contrast agents ( $T_2$  contrast agents).<sup>72–74</sup> Figure 7C, D shows  $T_1$ - and  $T_2$ -weighted MR images of agarose gel containing different concentrations of NCP-1 as compared to control (agarose gel). In  $T_1$ -weighted MR imaging, the intensity of the image increases with the concentration of contrast materials while MR intensity decreases in the  $T_2$ -weighted image. These results can be explained on the basis of hydrophobicity of NCP-1. As shown in Figure 2B, Gd<sup>III</sup> ions with coordinated water molecules are aligned in the hydrophobic pore surface derived from the interdigititation of the alkyl chains.  $T_1$  contrast agents require immediate contact with water molecules to accelerate  $T_1$  relaxation through spin-lattice interaction. However, hydrophobicity at the pore window of NCP-1 restricts outer water molecules to enter pore channels and interact with  $\text{Gd}^{III}$  ion which results in low longitudinal relaxivity ( $r_1$ ). However, transverse ( $T_2$ ) relaxation (spin–spin) of coordinated water molecules is greatly shortened due to their strong interaction with  $\text{Gd}^{III}$  center resulting in high transverse relaxivity ( $r_2$ ).

**Nitroaromatic Sensing.** Unique luminescence and porous properties of porous coordination polymers have been explored for sensory applications.<sup>19–21</sup> Inherent porosity could accommodate analyte molecules inside the framework, and such analyte molecules would alter the emission properties based on host guest interactions with chromophoric linker. Although several PCPs have been explored as sensor materials in bulk scale, very few attempts have been made for NCPs. High surface area to volume ratio, less diffusion barrier, and easy processable nature of NCPs would be advantageous over bulk PCPs. Presence of nanorod-like morphology, strong linker-based luminescence, and permanent porosity of NCP-1 encouraged us to study its potential for sensing applications. Fluorescence behavior of NCP-1 in the presence of different analytes has been studied. No considerable changes in luminescence of NCP-1 are observed in the presence of analytes such as benzene, xylene, and chlorobenzene. Interestingly, significant quenching of fluorescence was observed in case of nitro derivatives like nitromethane, nitrobenzene, and *o*-nitrophenol. Supporting Information

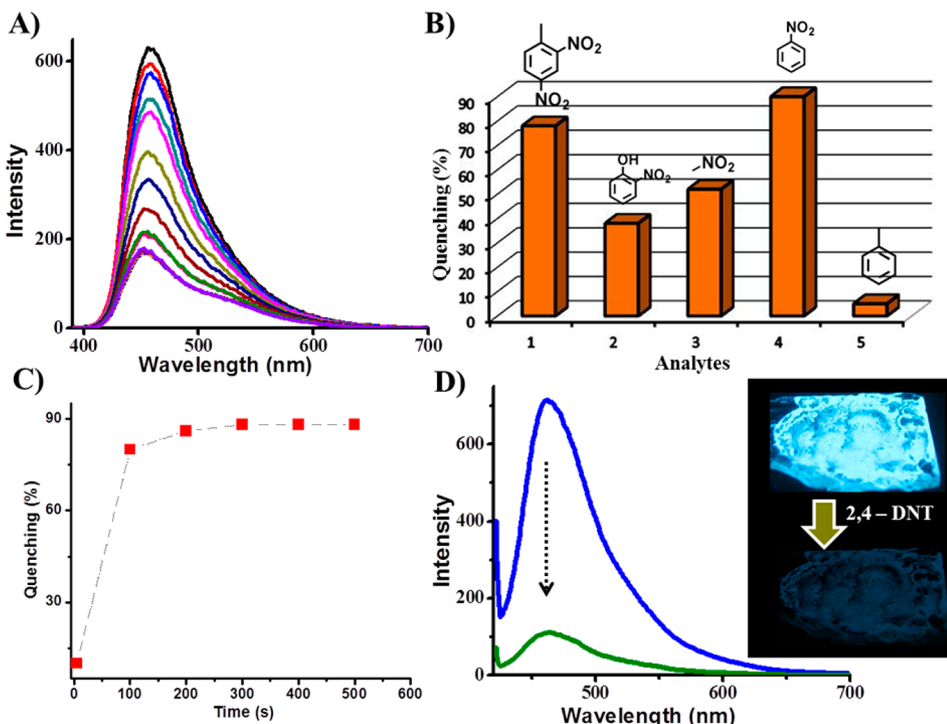


**Figure 8.** (A) Fluorescence quenching of NCP-1, dispersed in ethanol in the presence of 2,4-DNT, (B) bar diagram showing extent of fluorescence quenching of NCP-1 with different analytes, and (C), (D) fluorescence quenching behavior of NCP-1 coated on quartz ( $0.7 \times 1.2$  cm) glass after exposure to 2,4-DNT vapors with time. Inset: enlarged images of quartz glass plate coated with NCP-1 under UV light before and after 2,4-DNT exposure.

Figure S10 shows the fluorescence quenching with addition of different volumes of nitromethane ( $1 \times 10^{-3}$  M), *o*-nitrophenol ( $3 \times 10^{-3}$  M), nitrobenzene ( $1 \times 10^{-4}$  M), and 2,4-DNT ( $4 \times 10^{-5}$  M) (Figure 8A, B) analyte to NCP-1 dispersed in ethanol. However, when saturated vapors of 2,4-DNT are exposed to NCP-1 coated on a quartz glass, abrupt quenching of fluorescence was observed (Figure 8C, D). Within 100 s of exposure to 2,4-DNT, emission of NCP-1 is quenched about 80% and saturated after 300 s. This quick response may be due to diffusion of DNT molecules into coordination polymer at a faster rate in the vapor phase. Among nitroaromatics, nitrobenzene showed fast quenching in solution phase of analyte. The strong quenching of NCP-1 fluorescence could be attributed to photoinduced charge transfer from excited state of NCPs to electron-deficient nitro derivatives. In addition, the presence of large surface area to volume ratio of nanorods, microporosity, and less diffusion barrier of NCPs are believed to enhance the efficiency of fluorescence quenching.

## CONCLUSIONS

In conclusion, a new porous nanoscale coordination polymer based on Gd<sup>III</sup> metal ion and luminescent OPE–dicarboxylic acid has been successfully synthesized. Elegant design of OPEA with long alkyl chains on both ends results in interdigititation of 1D coordination chains assembled with Gd<sup>III</sup> and OPEA resulting in a supramolecular 3D porous structure in polar solvent. CO<sub>2</sub> adsorption isotherms, electron microscopy images, and diffraction measurements validate the proposed interdigitated structure with permanent microporosity and long-range structural ordering of NCPs. Significant hydrolytic stability, low toxicity, and self-luminescence features of NCP-1 have been successfully explored for cell internalization and optical imaging applications. Further, the presence of a large

number of Gd<sup>III</sup> centers in NCP-1 resulted in enhanced transverse relaxivity of water and showed to be a potential negative contrast agent (T<sub>2</sub> contrast agent). Furthermore, NCP-1 has been explored for sensing of nitroaromatic derivatives. To the best of our knowledge, luminescent NCPs having permanent microporosity have never been reported for multimodal imaging applications. These nanostructures with easy transferability onto solid substrates and descent sensing capabilities would pave new pathways to fabricate functional hybrid materials for optoelectronic applications.

## ASSOCIATED CONTENT

### Supporting Information

Synthetic scheme, <sup>1</sup>H NMR of OPEA, EDAX, IR spectra, and TGA curve of assynthesized NCP-1, PXRD pattern of NCP-1 compared with dehydrated and PBS incubated NCP-1, absorbance, emission spectra of NCP-1, and fluorescence quenching in the presence of nitroaromatics. This material is available free of charge via the Internet at <http://pubs.acs.org>.

## AUTHOR INFORMATION

### Corresponding Author

\*Tel.: +91-80-22082826. E-mail: tmaji@jncasr.ac.in.

### Notes

The authors declare no competing financial interest.

## ACKNOWLEDGMENTS

We thank Prof. C. N. R. Rao for his support and encouragement. We acknowledge Selvi (FESEM) and Usha (TEM) for microscopic measurements. V.M.S. thanks CSIR (government of India) for fellowship. T.K.M. gratefully acknowledges Sheikh Saqr fellowship.

## REFERENCES

- (1) Zhou, H.-C.; Long, J. R.; Yaghi, O. M. Introduction to Metal–Organic Frameworks. *Chem. Rev.* **2012**, *112*, 673–674.
- (2) Kitagawa, S.; Kitaura, R.; Noro, S. Functional Porous Coordination Polymers. *Angew. Chem., Int. Ed.* **2004**, *43*, 2334–2375.
- (3) Perry, J. J. I. V.; Perman, J. A.; Zaworotko, M. J. Design and Synthesis of Metal–Organic Frameworks Using Metal–Organic Polyhedra as Supramolecular Building Blocks. *Chem. Soc. Rev.* **2009**, *38*, 1400–1417.
- (4) James, S. L. Metal–Organic Frameworks. *Chem. Soc. Rev.* **2003**, *32*, 276–288.
- (5) Wang, Z.; Cohen, S. M. Postsynthetic Modification of Metal–Organic Frameworks. *Chem. Soc. Rev.* **2009**, *38*, 1315–1329.
- (6) Morris, W.; Doonan, C. J.; Furukawa, H.; Banerjee, R.; Yaghi, O. M. Crystals as Molecules: Postsynthesis Covalent Functionalization of Zeolitic Imidazolate Frameworks. *J. Am. Chem. Soc.* **2008**, *130*, 12626–12627.
- (7) Liu, B.; Ma, M.; Zacher, D.; Betard, A.; Yusenko, K.; Metzler-Nolte, N.; Woell, C.; Fischer, R. A. Chemistry of SURMOFs: Layer-Selective Installation of Functional Groups and Post-Synthetic Covalent Modification Probed by Fluorescence Microscopy. *J. Am. Chem. Soc.* **2011**, *133*, 1734–1737.
- (8) Sumida, K.; Rogow, D. L.; Mason, J. A.; McDonald, T. M.; Bloch, E. D.; Herm, Z. R.; Bae, T.-H.; Long, J. R. Carbon Dioxide Capture in Metal–Organic Frameworks. *Chem. Rev.* **2012**, *112*, 724–781.
- (9) Ma, S.; Zhou, H.-C. Gas Storage in Porous Metal–Organic Frameworks for Clean Energy Applications. *Chem. Commun.* **2010**, *46*, 44–53.
- (10) Murray, L. J.; Dinca, M.; Long, J. R. Hydrogen Storage in Metal–Organic Frameworks. *Chem. Soc. Rev.* **2009**, *38*, 1294–1314.
- (11) Liu, J.; Thallapally, P. K.; McGrail, B. P.; Brown, D. R.; Liu, J. Progress in Adsorption-Based CO<sub>2</sub> Capture by Metal–Organic Frameworks. *Chem. Soc. Rev.* **2012**, *41*, 2308–2322.
- (12) Vaithyanathan, R.; Iremonger, S. S.; Shimizu, G. K. H.; Boyd, P. G.; Alavi, S.; Woo, T. K. Competition and Cooperativity in Carbon Dioxide Sorption by Amine-Functionalized Metal–Organic Frameworks. *Angew. Chem., Int. Ed.* **2012**, *51*, 1826–1829.
- (13) Kanoo, P.; Mostafa, G.; Matsuda, R.; Kitagawa, S.; Maji, T. K. A Pillared-Bilayer Porous Coordination Polymer with a 1D Channel and a 2D Interlayer Space, Showing Unique Gas and Vapor Sorption. *Chem. Commun.* **2011**, *47*, 8106–8108.
- (14) Li, J.-R.; Kuppler, R. J.; Zhou, H.-C. Selective Gas Adsorption and Separation in Metal–Organic Frameworks. *Chem. Soc. Rev.* **2009**, *38*, 1477–1504.
- (15) Jeazet, H. B. T.; Staudt, C.; Janiak, C. Metal–Organic Frameworks in Mixed-Matrix Membranes for Gas Separation. *Dalton Trans.* **2012**, *41*, 14003–14027.
- (16) Li, J.-R.; Ma, Y.; McCarthy, M. C.; Sculley, J.; Yu, J.; Jeong, H.-K.; Balbuena, P. B.; Zhou, H.-C. Carbon Dioxide Capture-Related Gas Adsorption and Separation in Metal–Organic Frameworks. *Coord. Chem. Rev.* **2011**, *255*, 1791–1823.
- (17) Bae, T.-H.; Lee, J. S.; Qiu, W.; Koros, W. J.; Jones, C. W.; Nair, S. A. High-Performance Gas-Separation Membrane Containing Submicrometer-Sized Metal–Organic Framework Crystals. *Angew. Chem., Int. Ed.* **2010**, *49*, 9863–9866.
- (18) Xiong, S.; He, Y.; Krishna, R.; Chen, B.; Wang, Z. Metal–Organic Framework with Functional Amide Groups for Highly Selective Gas Separation. *Cryst. Growth Des.* **2013**, *13*, 2670–2674.
- (19) Allendorf, M. D.; Houk, R. J. T.; Andruszkiewicz, L.; Talin, A. A.; Pikarsky, J.; Choudhury, A.; Gall, K. A.; Hesketh, P. J. Stress-Induced Chemical Detection Using Flexible Metal–Organic Frameworks. *J. Am. Chem. Soc.* **2008**, *130*, 14404–14405.
- (20) Chen, L.; Tan, K.; Lan, Y.-Q.; Li, S.-L.; Shao, K.-Z.; Su, Z.-M. Unusual Microporous Polycatenane-Like Metal–Organic Frameworks for the Luminescent Sensing of Ln<sup>3+</sup> Cations and Rapid Adsorption of Iodine. *Chem. Commun.* **2012**, *48*, 5919–5921.
- (21) Chen, B.; Wang, L.; Xiao, Y.; Fronczek, F. R.; Xue, M.; Cui, Y.; Qian, G. A Luminescent Metal–Organic Framework with Lewis Basic Pyridyl Sites for the Sensing of Metal Ions. *Angew. Chem., Int. Ed.* **2009**, *48*, 500–503.
- (22) Horcajada, P.; Serre, C.; Maurin, G.; Ramsahye, N. A.; Balas, F.; Vallet-Regi, M.; Sebban, M.; Taulelle, F.; Ferey, G. Flexible Porous Metal–Organic Frameworks for a Controlled Drug Delivery. *J. Am. Chem. Soc.* **2008**, *130*, 6774–6780.
- (23) McKinlay, A. C.; Morris, R. E.; Horcajada, P.; Ferey, G.; Gref, R.; Couvreur, P.; Serre, C. BioMOFs: Metal–Organic Frameworks for Biological and Medical Applications. *Angew. Chem., Int. Ed.* **2010**, *49*, 6260–6266.
- (24) Huxford, R. C.; Della Rocca, J.; Lin, W. Metal–Organic Frameworks as Potential Drug Carriers. *Curr. Opin. Chem. Biol.* **2010**, *14*, 262–268.
- (25) Horcajada, P.; Gref, R.; Baati, T.; Allan, P. K.; Maurin, G.; Couvreur, P.; Ferey, G.; Morris, R. E.; Serre, C. Metal–Organic Frameworks in Biomedicine. *Chem. Rev.* **2012**, *112*, 1232–1268.
- (26) Chandler, B. D.; Cramb, D. T.; Shimizu, G. K. H. Microporous Metal–Organic Frameworks Formed in a Stepwise Manner from Luminescent Building Blocks. *J. Am. Chem. Soc.* **2006**, *128*, 10403–10412.
- (27) Suresh, V. M.; George, S. J.; Maji, T. K. MOF Nano-Vesicles and Toroids: Self-Assembled Porous Soft-Hybrids for Light Harvesting. *Adv. Funct. Mater.* **2013**, *23*, 5585–5590.
- (28) Takashima, Y.; Martinez Martinez, V.; Furukawa, S.; Kondo, M.; Shimomura, S.; Uehara, H.; Nakahama, M.; Sugimoto, K.; Kitagawa, S. Synthesis of Hexagonal Close-Packed Gold Nanostructures. *Nat. Commun.* **2011**, *2*.
- (29) Thallapally, P. K.; Fernandez, C. A.; Motkuri, R. K.; Nune, S. K.; Liu, J.; Peden, C. H. F. Micro and Mesoporous Metal–Organic Frameworks for Catalysis Applications. *Dalton Trans.* **2010**, *39*, 1692–1694.
- (30) Lee, J.; Farha, O. K.; Roberts, J.; Scheidt, K. A.; Nguyen, S. T.; Hupp, J. T. Metal–Organic Framework Materials as Catalysts. *Chem. Soc. Rev.* **2009**, *38*, 1450–1459.
- (31) Ma, L.; Abney, C.; Lin, W. Enantioselective Catalysis with Homochiral Metal–Organic Frameworks. *Chem. Soc. Rev.* **2009**, *38*, 1248–1256.
- (32) Song, F.; Wang, C.; Falkowski, J. M.; Ma, L.; Lin, W. Isoreticular Chiral Metal–Organic Frameworks for Asymmetric Alkene Epoxidation: Tuning Catalytic Activity by Controlling Framework Catenation and Varying Open Channel Sizes. *J. Am. Chem. Soc.* **2010**, *132*, 15390–15398.
- (33) Chen, B.; Xiang, S.; Qian, G. Metal–Organic Frameworks with Functional Pores for Recognition of Small Molecules. *Acc. Chem. Res.* **2010**, *43*, 1115–1124.
- (34) Uemura, T.; Yanai, N.; Kitagawa, S. Polymerization Reactions in Porous Coordination Polymers. *Chem. Soc. Rev.* **2009**, *38*, 1228–1236.
- (35) Wen, L.; Zhou, L.; Zhang, B.; Meng, X.; Qu, H.; Li, D. Multifunctional Amino-Decorated Metal–Organic Frameworks: Non-linear-Optic, Ferroelectric, Fluorescence Sensing, and Photocatalytic Properties. *J. Mater. Chem.* **2012**, *22*, 22603–22609.
- (36) Vilela, S. M. F.; Ananias, D.; Gomes, A. C.; Valente, A. A.; Carlos, L. D.; Cavaleiro, J. A. S.; Rocha, J.; Tome, J. P. C.; Almeida Paz, F. A. Multifunctional Metal–Organic Frameworks Assembled from a Tripodal Organic Linker. *J. Mater. Chem.* **2012**, *22*, 18354–18371.
- (37) Mohapatra, S.; Rajeswaran, B.; Chakraborty, A.; Sundaresan, A.; Maji, T. K. Bimodal Magneto-Luminescent Dysprosium (Dy<sup>III</sup>)–Potassium (K<sup>+</sup>)–Oxalate Framework: Magnetic Switchability with High Anisotropic Barrier and Solvent Sensing. *Chem. Mater.* **2013**, *25*, 1673–1679.
- (38) Hazra, A.; Kanoo, P.; Maji, T. K. High Heat of Hydrogen Adsorption and Guest-Responsive Magnetic Modulation in a 3D Porous Pillared-Layer Coordination Framework. *Chem. Commun.* **2011**, *47*, 538–540.
- (39) Jayaramulu, K.; Kanoo, P.; George, S. J.; Maji, T. K. Tunable Emission from a Porous Metal–Organic Framework by Employing an Excited-State Intramolecular Proton Transfer Responsive Ligand. *Chem. Commun.* **2010**, *46*, 7906–7908.

- (40) Kanoo, P.; Ghosh, A. C.; Cyriac, S. T.; Maji, T. K. A Metal–Organic Framework with Highly Polar Pore Surfaces: Selective CO<sub>2</sub> Adsorption and Guest-Dependent On/Off Emission Properties. *Chem.—Eur. J.* **2012**, *18*, 237–244.
- (41) Guo, Z.; Cao, R.; Wang, X.; Li, H.; Yuan, W.; Wang, G.; Wu, H.; Li, J. A Multifunctional 3D Ferroelectric and NLO-Active Porous Metal–Organic Framework. *J. Am. Chem. Soc.* **2009**, *131*, 6894–6895.
- (42) Maspoch, D.; Ruiz-Molina, D.; Wurst, K.; Domingo, N.; Cavallini, M.; Biscarini, F.; Tejada, J.; Rovira, C.; Veciana, J. A Nanoporous Molecular Magnet with Reversible Solvent-Induced Mechanical and Magnetic Properties. *Nat. Mater.* **2003**, *2*, 190–195.
- (43) Allendorf, M. D.; Bauer, C. A.; Bhakta, R. K.; Houk, R. J. T. Luminescent Metal–Organic Frameworks. *Chem. Soc. Rev.* **2009**, *38*, 1330–1352.
- (44) Umemura, A.; Diring, S.; Furukawa, S.; Uehara, H.; Tsuruoka, T.; Kitagawa, S. Morphology Design of Porous Coordination Polymer Crystals by Coordination Modulation. *J. Am. Chem. Soc.* **2011**, *133*, 15506–15513.
- (45) Xu, H.; Liu, F.; Cui, Y.; Chen, B.; Qian, G. A Luminescent Nanoscale Metal–Organic Framework for Sensing of Nitroaromatic Explosives. *Chem. Commun.* **2011**, *47*, 3153–3155.
- (46) Della Rocca, J.; Liu, D.; Lin, W. Nanoscale Metal–Organic Frameworks for Biomedical Imaging and Drug Delivery. *Acc. Chem. Res.* **2011**, *44*, 957–968.
- (47) Carne, A.; Carbonell, C.; Imaz, I.; Maspoch, D. Nanoscale Metal–Organic Materials. *Chem. Soc. Rev.* **2011**, *40*, 291–305.
- (48) Imaz, I.; Hernando, J.; Ruiz-Molina, D.; Maspoch, D. Metal–Organic Spheres as Functional Systems for Guest Encapsulation. *Angew. Chem., Int. Ed.* **2009**, *48*, 2325–2329.
- (49) Nishiyabu, R.; Hashimoto, N.; Cho, T.; Watanabe, K.; Yasunaga, T.; Endo, A.; Kaneko, K.; Niidome, T.; Murata, M.; Adachi, C.; et al. Nanoparticles of Adaptive Supramolecular Networks Self-Assembled from Nucleotides and Lanthanide Ions. *J. Am. Chem. Soc.* **2009**, *131*, 2151–2158.
- (50) deKrafft, K. E.; Boyle, W. S.; Burk, L. M.; Zhou, O. Z.; Lin, W. Zr- and Hf-Based Nanoscale Metal–Organic Frameworks as Contrast Agents for Computed Tomography. *J. Mater. Chem.* **2012**, *22*, 18139–18144.
- (51) Rieter, W. J.; Taylor, K. M. L.; Lin, W. Surface Modification and Functionalization of Nanoscale Metal–Organic Frameworks for Controlled Release and Luminescence Sensing. *J. Am. Chem. Soc.* **2007**, *129*, 9852–9853.
- (52) Horcajada, P.; Chalati, T.; Serre, C.; Gillet, B.; Sebrie, C.; Baati, T.; Eubank, J. F.; Heurtaux, D.; Clayette, P.; Kreuz, C.; et al. Porous Metal–Organic-Framework Nanoscale Carriers as a Potential Platform for Drug Delivery and Imaging. *Nat. Mater.* **2010**, *9*, 172.
- (53) Otsubo, K.; Haraguchi, T.; Sakata, O.; Fujiwara, A.; Kitagawa, H. Step-by-Step Fabrication of a Highly Oriented Crystalline Three-Dimensional Pillared-Layer-Type Metal–Organic Framework Thin Film Confirmed by Synchrotron X-ray Diffraction. *J. Am. Chem. Soc.* **2012**, *134*, 9605–9608.
- (54) Rieter, W. J.; Pott, K. M.; Taylor, K. M. L.; Lin, W. Nanoscale Coordination Polymers for Platinum-Based Anticancer Drug Delivery. *J. Am. Chem. Soc.* **2008**, *130*, 11584–11585.
- (55) Taylor, K. M. L.; Rieter, W. J.; Lin, W. Manganese-Based Nanoscale Metal–Organic Frameworks for Magnetic Resonance Imaging. *J. Am. Chem. Soc.* **2008**, *130*, 14358–14359.
- (56) Shekhah, O.; Hirai, K.; Wang, H.; Uehara, H.; Kondo, M.; Diring, S.; Zacher, D.; Fischer, R. A.; Sakata, O.; Kitagawa, S.; et al. MOF-on-MOF Heteroepitaxy: Perfectly Oriented [Zn<sub>2</sub>(ndc)<sub>2</sub>(dabco)]<sub>n</sub> Grown on [Cu<sub>2</sub>(ndc)<sub>2</sub>(dabco)]<sub>n</sub> Thin Films. *Dalton Trans.* **2011**, *40*, 4954–4958.
- (57) Liu, B.; Shekhah, O.; Arslan, H. K.; Liu, J.; Woell, C.; Fischer, R. A. Enantiopure Metal–Organic Framework Thin Films: Oriented SURMOF Growth and Enantioselective Adsorption. *Angew. Chem., Int. Ed.* **2012**, *51*, 807–810.
- (58) Bradshaw, D.; Garai, A.; Huo, J. Metal–Organic Framework Growth at Functional Interfaces: Thin Films and Composites for Diverse Applications. *Chem. Soc. Rev.* **2012**, *41*, 2344–2381.
- (59) Taylor-Pashow, K. M. L.; Della Rocca, J.; Xie, Z.; Tran, S.; Lin, W. Postsynthetic Modifications of Iron-Carboxylate Nanoscale Metal–Organic Frameworks for Imaging and Drug Delivery. *J. Am. Chem. Soc.* **2009**, *131*, 14261–14263.
- (60) Taylor, K. M. L.; Jin, A.; Lin, W. Surfactant-Assisted Synthesis of Nanoscale Gadolinium Metal–Organic Frameworks for Potential Multimodal Imaging. *Angew. Chem., Int. Ed.* **2008**, *47*, 7722–7725.
- (61) Li, Q.; Rukavishnikov, A. V.; Petukhov, P. A.; Zaikova, T. O.; Jin, C. S.; Keana, J. F. W. Nanoscale Tripodal 1,3,5,7-Tetrasubstituted Adamantanes for AFM Applications. *J. Org. Chem.* **2003**, *68*, 4862–4869.
- (62) Mangalam, A.; Gilliard, R. J., Jr.; Hanley, J. M.; Parker, A. M.; Smith, R. C. Metal Ion Detection by Luminescent 1,3-Bis-(dimethylaminomethyl)phenyl Receptor-Modified Chromophores and Cruciforms. *Org. Biol. Chem.* **2010**, *8*, 5620–5627.
- (63) Chatterjee, S.; Mizar, P.; Cassel, R.; Neidl, R.; Selvi, B. R.; Mohankrishna, D. V.; Vedamurthy, B. M.; Schneider, A.; Bousiges, O.; Mathis, C.; et al. A Novel Activator of CBP/p300 Acetyltransferases Promotes Neurogenesis and Extends Memory Duration in Adult Mice. *J. Neurosci.* **2013**, *33*, 10698–10712.
- (64) Dutta, A.; Mondal, J.; Patra, A. K.; Bhaumik, A. Synthesis and Temperature-Induced Morphological Control in a Hybrid Porous Iron-Phosphonate Nanomaterial and Its Excellent Catalytic Activity in the Synthesis of Benzimidazoles. *Chem.—Eur. J.* **2012**, *18*, 13372–13378.
- (65) Wei, H.; Li, B.; Du, Y.; Dong, S.; Wang, E. Nucleobase–Metal Hybrid Materials: Preparation of Submicrometer-Scale, Spherical Colloidal Particles of Adenine-Gold(III) via a Supramolecular Hierarchical Self-Assembly Approach. *Chem. Mater.* **2007**, *19*, 2987–2993.
- (66) Noh, E.; Park, S.; Kang, S.; Lee, J. Y.; Jung, J. H. Remarkable Reinforcement of a Supramolecular Gel Constructed by Heteroditopic [18]Crown-6-Based Molecular Recognition. *Chem.—Eur. J.* **2013**, *19*, 2620–2627.
- (67) Lee, J. H.; Kang, S.; Lee, J. Y.; Jaworski, J.; Jung, J. H. Instant Visual Detection of Picogram Levels of Trinitrotoluene by Using Luminescent Metal–Organic Framework Gel-Coated Filter Paper. *Chem.—Eur. J.* **2013**, *19*, 16665–16671.
- (68) Yoosaf, K.; Ramesh, A. R.; George, J.; Suresh, C. H.; Thomas, K. G. Functional Control on the 2D Self-Organization of Phenylethylenylenes. *J. Phys. Chem. C* **2009**, *113*, 11836–11843.
- (69) Battistini, E.; Gianolio, E.; Gref, R.; Couvreur, P.; Fuzerova, S.; Othman, M.; Aime, S.; Badet, B.; Durand, P. High-Relaxivity Magnetic Resonance Imaging (MRI) Contrast Agent Based on Supramolecular Assembly between a Gadolinium Chelate, a Modified Dextran, and Poly- $\beta$ -cyclodextrin. *Chem.—Eur. J.* **2008**, *14*, 4551–4561.
- (70) Chaturbedy, P.; Chatterjee, S.; Selvi, R. B.; Bhat, A.; Kavitha, M. K.; Tiwari, V.; Patel, A. B.; Kundu, T. K.; Maji, T. K.; Eswaramoothy, M. Multifunctional Carbon Nanospheres with Magnetic and Luminescent Probes: Probable Brain Theranostic Agents. *J. Mater. Chem. B* **2013**, *1*, 939–945.
- (71) Qin, J.; Laurent, S.; Jo, Y. S.; Roch, A.; Mikhaylova, M.; Bhujwalla, Z. M.; Muller, R. N.; Muhammed, M. A High-Performance Magnetic Resonance Imaging T<sub>2</sub> Contrast Agent. *Adv. Mater.* **2007**, *19*, 1874–1878.
- (72) Richard, C.; Doan, B.-T.; Beloeil, J.-C.; Bessodes, M.; Toth, E.; Scherman, D. Noncovalent Functionalization of Carbon Nanotubes with Amphiphilic Gd<sup>3+</sup> Chelates: Toward Powerful T<sub>1</sub> and T<sub>2</sub> MRI Contrast Agents. *Nano Lett.* **2008**, *8*, 232–236.
- (73) Lim, C.-K.; Singh, A.; Heo, J.; Kim, D.; Lee, K. E.; Jeon, H.; Koh, J.; Kwon, I.-C.; Kim, S. Gadolinium-Coordinated Elastic Nanogels for in Vivo Tumor Targeting and Imaging. *Biomaterials* **2013**, *34*, 6846–6852.
- (74) Casula, M. F.; Floris, P.; Innocenti, C.; Lascialfari, A.; Marinone, M.; Corti, M.; Sperling, R. A.; Parak, W. J.; Sangregorio, C. Magnetic Resonance Imaging Contrast Agents Based on Iron Oxide Superparamagnetic Ferrofluids. *Chem. Mater.* **2010**, *22*, 1739–1748.